Hindawi
Advances in Materials Science and Engineering
Volume 2022, Article ID 1231843, 11 pages
https://doi.org/10.1155/2022/1231843

Research Article

Experimental Investigation to Analyze the Mechanical and Microstructure Properties of 310 SS Performed by TIG Welding

Ashish Goyal,[1] **Hardik Kapoor**,[1] **Lade Jayahari**,[2] **Kuldeep K Saxena**,[3] **N. Ummal Salmaan**,[4] **and Kahtan A. Mohammed**[5]

[1]*Department of Mechanical Engineering, Manipal University Jaipur, Rajasthan 303007, India*
[2]*Department of Mechanical Engineering, KG Reddy College of Engineering & Technology, Hyderabad, India*
[3]*Department of Mechanical Engineering, GLA University, Mathura 281406, UP, India*
[4]*Department of Automotive Engineering, Aksum University, Aksum, Ethiopia*
[5]*Department of Medical Physics, Hilla University College, Babylon, Iraq*

Correspondence should be addressed to N. Ummal Salmaan; ummalsalmaan90@gmail.com

Received 15 June 2022; Revised 5 July 2022; Accepted 12 July 2022; Published 20 August 2022

Academic Editor: J. T. Winowlin Jappes

In present experimental work, 310 SS alloy has been welded by the TIG welding using design of experiment and grey relation optimization techniques. The input parameters, i.e., welding current, welding gas flow rate, and welding voltage, have been selected to perform the TIG welding. The same filler material was used during the welding process to investigate the mechanical and microstructure properties. The design of experiment and grey relation optimization techniques were used to optimize the effect on hardness and tensile strength of the welded joints. The experiments were performed as per the L9 orthogonal array obtained by the design of experiment methodology. The 65 A, 12 V, and 7.5 gas flow rate optimum setting of input parameters provides the better results for the effective hardness and tensile strength. The most significant parameters, i.e., welding current with 84.93% and welding voltage with 65.09%, were obtained for hardness and tensile strength, respectively.

1. Introduction

The high strength low alloy (HSLA) steels have become widely popular in fabrication of various structures for critical and noncritical applications due to reasonable economy and high allowable design stresses. Sarkar and Kakoty performed welding for joining of the bell metal parts. The multiobjective algorithm has been adopted to solve the regression equation. Also, mechanical and microstructure properties have also been analyzed in this study [1]. Sathish et al. reported that wrought aluminum AA8006 was welded by tungsten inert gas welding for the industrial applications. The welding speed, base current, and peak current had considered a process parameter and the surface hardness, strengths for standing tensile, and impact loading have been analyzed [2]. Chuaiphan and Srijaroenpramong revealed the joining of dissimilar metals AISI 205 and AISI 216 stainless by using TIG welding process. It was found that range of welding speed of 1–3.5 gives the defect-free and complete weld bead. This study will be useful for various industrial applications [3]. Sharma et al. performed experiments on TIG welding to join the SS202 metal. The electrode diameter, shielding gas, gas flow rate, welding current, and groove angle were considered as input parameters and the effect of these parameters was analyzed on hardness and tensile strength. The obtained results were compared with estimated mean value and the results were lying within ±5% [4]. Pavan et al. revealed welding of 6.5 mm thick Inconel 625 alloy plate. The results had been investigated by using grey relational analysis (GRA) and technique for order preference by similarity to ideal solution. It was found that the optimal level is at 300 A current, 90 mm/min torch travel speed, and 5 mm arc gap which provide the best value to obtain the good results [5]. Wan et al. examined tensile properties of 2219-T8 aluminum alloy for large propellent tanks manufacturing. The tensile strength coefficient of 70% and

4% elongation was achieved with design of experiment methodology [6]. Azadi Moghaddam and Kolahan evaluated the effect of welding current, welding speed, and welding gap for the fabrication of AISI316L austenitic stainless steel. The orthogonal array Taguchi, regression model, and analysis of variance have been adopted to optimize the parameters. The SiO_2 nano particle has been used for activating the flus. The authors suggested that the obtained model is effective in modelling and optimization of the A-TIG welding [7]. Pandya et al. revealed the tungsten inert gas welding for the stainless-steel metal. The authors have also concluded that activated TIG increases weld penetration up to 1.504 times in a single pass [8]. Balaram Naik and Chennakeshava Reddy proposed a model to reduce the errors and enhance the working of TIG welding process. Experiments performed on duplex stainless steel 2205b and also Taguchi and ANOVA analysis have been adopted to find the optimal values. Neural network model has been coupled with the optimization techniques to increase the tensile strength, hardness, and depth of weld [9]. Chuaiphan and Srijaroenpramong joined AISI 205 and AISI 216 stainless steel dissimilar metals by TIG welding. The ER307 filler metal has been used for welding purpose. Also, microstructure analysis was performed on the welded joints. It was concluded that the obtained weld bead is complete and without any defects, and microstructure was found narrower when welding at higher speeds [3]. Ragavendran et al. investigated the effect on the response during the welding by hybrid laser and TIG welding. The welding operation was performed in 316LN austenitic stainless steel. The effect had been investigated for weld bead width, weld cross-sectional area, and depth of penetration with response surface methodology. The good agreement has also been observed for the measured and predicted values [10]. Vidyarthy et al. studied the relation between the A-TIG welding process parameters and the response such as welding current, welding speed, and flux coating density by using the response surface methodology (RSM). It was found that the welding current is the most significant parameter that affects the weld bead geometry [11]. Vasantharaja and Vasudevan selected the optimum values during the welding by A-TIG welding process by response surface methodology. The numerical and graphical optimization was performed to identify the optimum values for the welding parameters [12]. Pamnani et al. performed experiments on DMR249A steel for aircraft and ships. The good depth of penetration was obtained by this process, and this was achieved by the design of experiment and RSM methodology [13]. Singh et al. studied the effect of vibratory welding process on mild steel plated for fabrication of butt weld. The microhardness and microstructure were also studied in this work. It has been found that the hardness value was enhanced during the vibratory condition compared to conventional process [14]. Magudeeswaran et al. revealed the identification of the desirable aspect ratio for the DSS joints by using A-TIG welding process. The ANOVA and pooled ANOVA techniques were adopted to identify the significant parameters of experiments. The authors concluded that optimized parameters were found to be within the acceptable range by ANOVA analysis [15]. Sivachidambaram and Balachandar investigated a solution to weld aluminum and aluminum composite by using optimized pulsed current parameters of pulsed current TIG, welding regression equations and empirical model has also established to identify the significant parameters [16]. Lugade and Deshmukh used SiO_2 flux powder to perform A-TIG welding on austenitic stainless steel (304L) with acetone. The process parameters i.e., electrode gap, welding current welding speed and gas flow rate was optimized by Taguchi's methodology. The optimum values of process parameters for weld specimens are, 1 mm electrode gap, 100 mm/min travel speed, 200 A welding current and 10 lit/min gas flow rate [17]. Adalarasan and Santhanakumar performed comparative studies by using the TIG and MIG welding on aluminum 6061 alloy. The desirability grey relation analysis was performed to optimize the process parameters of welding processes; also, the obtained results have been validated through the confirmation experiments [18]. Bello et al. studied the surface hardness for low alloy steel by using TIG welding process. The welding speed and welding voltage were found to be the most significant parameters that influenced the surface hardness. The obtained results have also been validated through the confirmation experiments [19]. Kiaee and Santhanakumar performed TIG welding on A516-Gr70 carbon steel to analyze the tensile strength. The optimized values of current, welding speed, and shielding gas flow rate have been identified by using RSM analysis. The obtained model can be used to predict the responses of TIG welded joints at 95% confidence level [20]. Rastkerdar et al. optimized the TIG welding process parameters to enhance the pitting corrosion resistance during welding of AA5083-H18 aluminum alloy. The authors concluded that pulses on time showed the significant effect on pitting corrosion resistance followed by pulse frequency, peak current, and base current [21]. Chakravarthy et al. performed Taguchi L16 experiments to analyze the effect of TIG parameters on tensile strength of PC GTAW of 70/30 CuNi alloy. The obtained values of optimum condition have also been investigated, i.e., 3.0 Hz for pulse frequency, 210 A for peak current, and 150 mm/min for base current [22]. Lin used Inconel l718 alloy to weld by TIG welding. The BPNN model has been developed for the TIG welding process parameters and Taguchi's and grey relational analysis has also been performed to identify the quality characteristics. The obtained results show the improvement in the weld bead and penetration of Inconel 718 alloy welds [23]. Some research put efforts to enhance the characteristics of process by using other statistical tools such as response surface methodology, fuzzy-ANFIS approach, and metaphor-less algorithms [24–28]. It was seen that most of the research work was carried out using the TIG welding but very few works have presented the optimization of the TIG welding parameters. In the present work, experiments have been performed on 310 SS alloy to identify the effect of TIG welding parameters on tensile strength and hardness. Also, optical analysis was performed to check the microstructure of the welded specimens. The design of experiment and grey relation analysis was used to optimize the process parameters of TIG welding.

2. Materials and Methodology

Tungsten inert gas welding (TIG) was performed in single pass with direct current electrode negative (DCEN). Argon gas is used as a shielding gas. The filler rod used is TIGINOX 308L. The TIGINOX 308L filler rod is suitable for the application for welding of piping system, tubes, and boilers in chemical and food processing industries. The welding current, gas flow rate, and voltage were considered as process parameters and the effects of these parameters were identified on tensile strength and hardness. The L9 orthogonal array was prepared by design of experiment (DOE) methodology. The welding is performed on 310 SS alloy. Figure 1 shows the total 9 pairs of specimens before the welding process.

Figure 2 shows the welding setup which is used for the experimental work. Table 1 shows the chemical composition of the base metal and filler materials which was used to perform the welding operation. Table 2 shows the used process parameters and their level for present experimental work. Figure 3 shows the welded joints after the TIG welding process.

2.1. Grey Relational Analysis. It is also abbreviated as GRA. It is utilized for finding the most optimal solution for given arrangements of parameters and for which parameter to optimize. Initially there is a need to define the input variables and response variables. Data can be collected for the same. The further step in GRA optimization is the normalization of response values on which optimization is to be carried out. For the smaller, better characteristics, the normalized value is obtained by

$$X_i = \left(\frac{x_{\max} - x_i}{x_{\max} - x_{\min}} \right). \quad (1)$$

The next step is to calculate the deviation sequence. Subtract corresponding normalized value from 1 as it is the maximum value.

$$\Delta = (X_i)_{\max} - \mathrm{X_i}. \quad (2)$$

Further, there is a need to calculate the grey relational coefficient. For that, there is a requirement of delta max and min.

$$\zeta_i(k) = \frac{\Delta_{\min} + \zeta \Delta_{\max}}{\Delta_i + \zeta \Delta_{\max}}. \quad (3)$$

The value of ζ is generally between 0 and 1. For the calculation purpose, the value of ζ can be used as 0.5. A further step is to calculate the grey relational grade. This is calculated by average of grey relational coefficients.

$$\gamma_i = \frac{1}{n} \sum \zeta_i(k). \quad (4)$$

Based on grey relational grade, these values are given rank. Larger value of grade means the observed values are close to the ideal normalized values. Parameters corresponding to the highest rank are the optimum solution.

3. Results and Discussion

Table 3 shows the orthogonal array which is used to perform the experiment and it also presents measurement of Vickers hardness test and tensile strength.

3.1. Microhardness Analysis. Hardness measurement was carried out at MRC Research Center, Jaipur. The Vickers microhardness tester was used for the measurement of hardness. The hardness has measured all the welded 9 specimens. Figure 4 shows visuals while performing the experiments.

After the measurement of hardness value, the obtained results were optimized by using the Minitab software and the obtained results have been discussed in the present section. Figure 5 shows the main effect plot obtained for the hardness test. It shows that the hardness of the weld has decreased steadily with the increase in welding current. The maximum hardness is obtained at a welding current of 65 A. Hardness increases from 170.5 HV to 172.5 HV at welding current of 65 A when current increases from 65 A to 75 A. It is a decrease to 168 HV. This decrease in hardness is owing to the weak solidification of the molten material. Even though there is a decrease in hardness of the welded joints with an increase in welding current, the travel speed of the filler has increased. At the same time, as the value of gas flow rate increases from 7.5 to 10 L/min, the hardness starts to increase. Similarly, an increase of gas flow rate from 7.5 lit/min to 10 lit/min has increased the hardness from 170 HV to 171 HV. When the gas flow rate increases from 10 lit/min to 12.5 lit/min, the hardness decreases from 171 HV to 170.5 HV. This increase in hardness is due to the increased supply of gas that has assisted the application of the higher volume of heat at the surface subsequent in poor solidification of the metal. Hardness decreases as the value of welding voltage increases. The gas flow rate has highly influenced this analysis, followed by current and voltage based on the obtained delta value and rank order.

The hardness is microstructural and heat input parameters dependent. The change in process parameters makes the heat flux intensity and metallurgical behavior vary, which further affects the defects formation in the weldment.

In the hardness test, the optimal parameters were obtained as current of 65 A, the gas flow rate of 10 lit/min, and voltage of 10 V.

Table 4 shows the obtained results by analysis of variance methodology. It shows that welding current was found to be the significant parameter because P value is less than 0.05 and it also shows the maximum percentage contribution of 84.93%. The gas flow rate and welding voltage were found to be nonsignificant parameters due to the P value being more than 0.05. Table 5 presents the model summary for the hardness analysis. It shows that the obtained value of R-sq(adj) is 93.96% and that of R-sq is 88.80% which shows the obtained result is within the range. Figure 6 shows the pie chart of % contribution of process parameters for hardness.

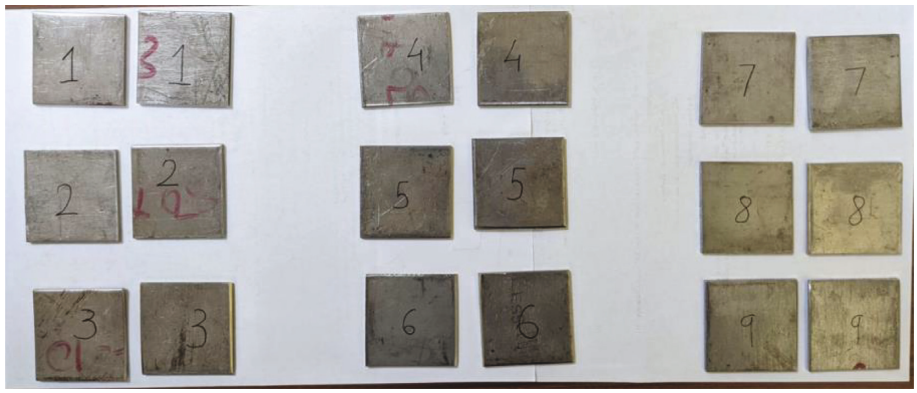

Figure 1: 9 pairs of 310 SS sheet specimen before welding (base metal).

Figure 2: TIG welding setup.

Table 1: Chemical composition materials.

Elements (%wt)	Base metal-310 SS	Filler material 308L
C	0.07	0.02
Mn	0.95	1.7
P	—	0.011
Cr	24–26	20
Mo	0.25	0.65
Ni	18.96	10
S	0.03	0.009
Si	1.58	0.32
Cu	—	0.68
Al	0.68	—

Table 2: Process parameters and their levels.

Parameters	Unit	Level 1	Level 2	Level 3
Welding current	A	65	70	75
Gas flow rate	L/min.	7.5	10	12.5
Welding voltage	V	10	12	14

Regression equation for microhardness is the following:

$$\text{Mmicrohardness} = 201.31 - 0.3933\,\text{I} + 0.0867\,\text{Q} - 0.3417\,\text{V}. \quad (5)$$

4. Tensile Stress Test

The tensile test was also performed at MRC Research Center, Jaipur. The obtained results were optimized by using the Minitab software. Figure 7 shows the specimens for the tensile test. The tensile strength of the specimen was determined by UTM (universal testing machine) as shown in Figure 8 and the corresponding stress-strain graph for specimen is presented in Figure 9. The influence of TIG welding process parameters on the strengths of weld was statistically analyzed by using Minitab 21 software, in which the experimental data are converted into mean to determine the optimal process parameters.

Figure 10 shows the main effects plot for means by the design of experiment methodology. The tensile strength of the weld has decreased steadily with the increase in welding current. The maximum tensile strength is obtained at a welding current of 65 A. A decrease in tensile strength from 472 MPa to 468 MPa is observed when the welding current increases from 65 A to 75 A. This decrease in tensile strength is owing to the penetration of a large amount of heat at the surface. The increased amount of heat produced at the weld surface leads to the decrease of tensile strength of the welded joint. Additionally, when the gas flow rate increases from 7.5 lit/min to 12.5 lit/min, the tensile strength has increased from 460 MPa to 478 MPa. This could be anticipated to an increased supply of gas, enabling the application of a higher amount of heat at the interface. This increased supply of heat at the surface caused better penetration of heat into the material. Likewise, as the welding voltage decreased from 10 V to 14 V, the tensile strength has decreased from 482 MPa to 458 MPa.

Table 6 shows the ANOVA analysis for tensile strength. The welding voltage was found to be the significant parameter and the welding current and gas flow rate were

Figure 3: Welded joint after the TIG welding.

Table 3: L9 orthogonal arrays and their responses.

Exp. no.	Current (A)	Gas flow rate (l/min)	Welding voltage (V)	Microhardness (HV)	Tensile strength (MPa)
1	65	7.5	10	173	472.6
2	65	10	12	172.4	472.1
3	65	12.5	14	171.8	470.8
4	70	7.5	12	170.2	467.6
5	70	10	14	170.7	457.5
6	70	12.5	10	171.4	488
7	75	7.5	14	167.3	444.4
8	75	10	10	169.5	491.9
9	75	12.5	12	168.6	469.7

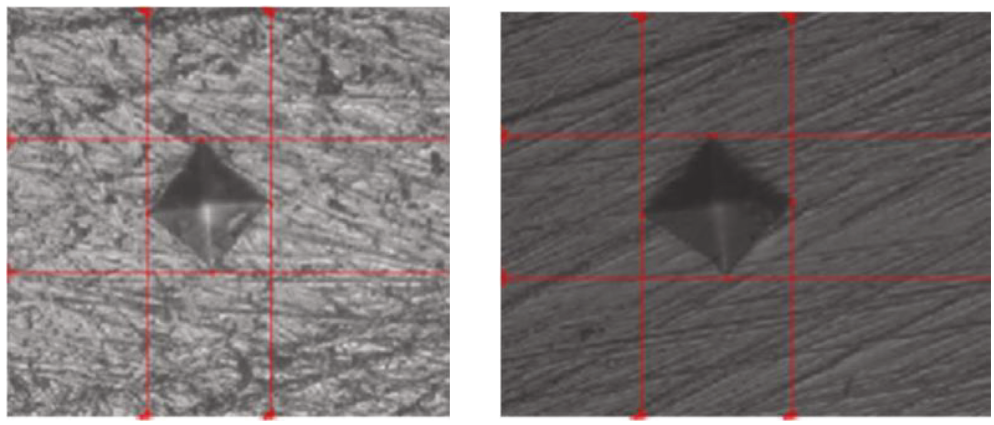

Figure 4: Visuals of the microhardness test.

found to be the nonsignificant parameters. Table 7 presents the model summary of tensile strength. Equation (2) shows the obtained regression equation for the present experimental work and R-sq(adj) is obtained as 77.14%. Figure 11 shows the pie chart of % contribution of process parameters for tensile strength.

Regression equation for tensile strength is as follows: tensile strength = $543.2 - 0.317I + 2.93Q - 6.65\,\mathrm{V}$ (6).

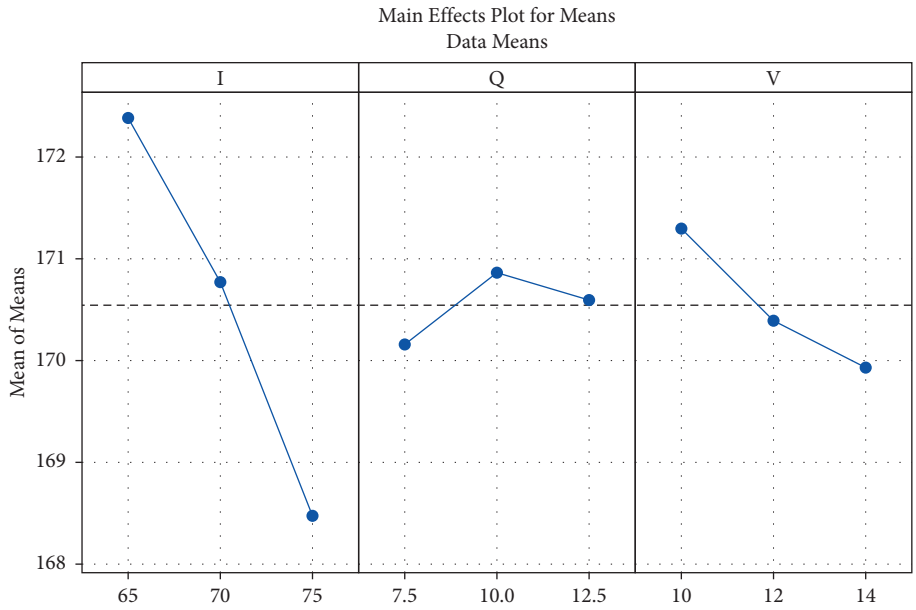

Figure 5: Main effects plot for means on microhardness.

Table 4: Analysis of variance for hardness.

Source	DF	Adj SS	Adj MS	F value	P value	% contribution
Regression	3	26.2900	8.7633	42.45	0.001	
Welding current	1	23.2067	23.2067	112.41	$P < 0.001$	84.93
Gas flow rate	1	0.2817	0.2817	1.36	0.295	1.031
Welding voltage	1	2.8017	2.8017	13.57	0.014	10.25
Error	5	1.0322	0.2064			3.77
Total	8	27.3222				

Table 5: Model summary (HV).

S	R-sq (%)	R-sq (adj) (%)	R-sq (pred) (%)
0.454362	96.22	93.96	88.80

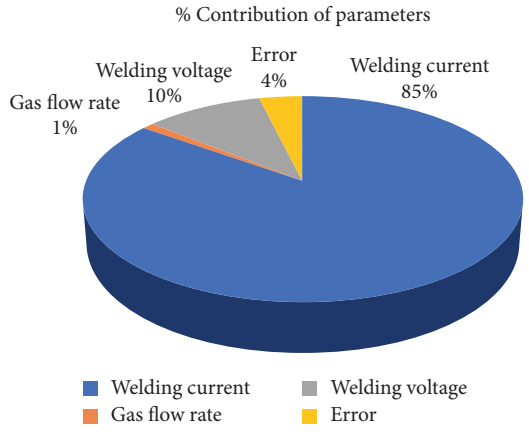

Figure 6: % contribution of parameters for hardness.

5. Grey Relation Analysis (GRA) for Hardness and Tensile Strength

Table 8 shows the obtained normalized values for the hardness and tensile strength for L9 orthogonal array. This value was obtained by using the grey relation analysis methodology.

The values GRC and GRG and the assigned ranks for all output responses are shown in Table 9. According to the ranking, the 1 experiment value has the highest grey relational grade value in Taguchi's L9 orthogonal array experimentation [29]. For other experiments, the rank is shown in Table 9.

5.1. Optical Analysis. The optical analysis was performed on the welded specimen. The specimens were carefully cut into small pieces and, after proper polishing by the picric acid, used for the microstructure analysis. The specimen was further cut into 10 mm width for tensile testing. Following the welding operation on the specimen, a microstructural analysis was carried out to determine the effect of welding

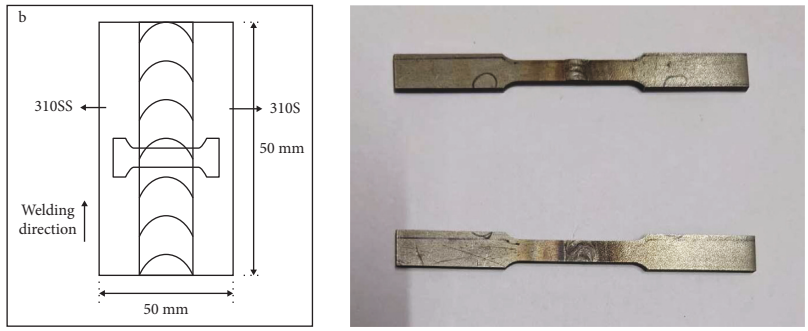

Figure 7: Specimens for the tensile test.

Figure 8: Specimen under a tensile test.

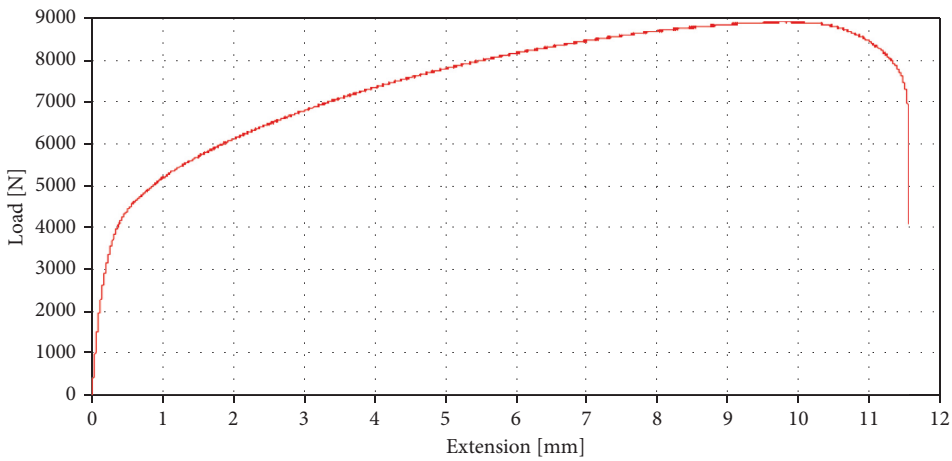

Figure 9: Stress-strain graph for the specimen.

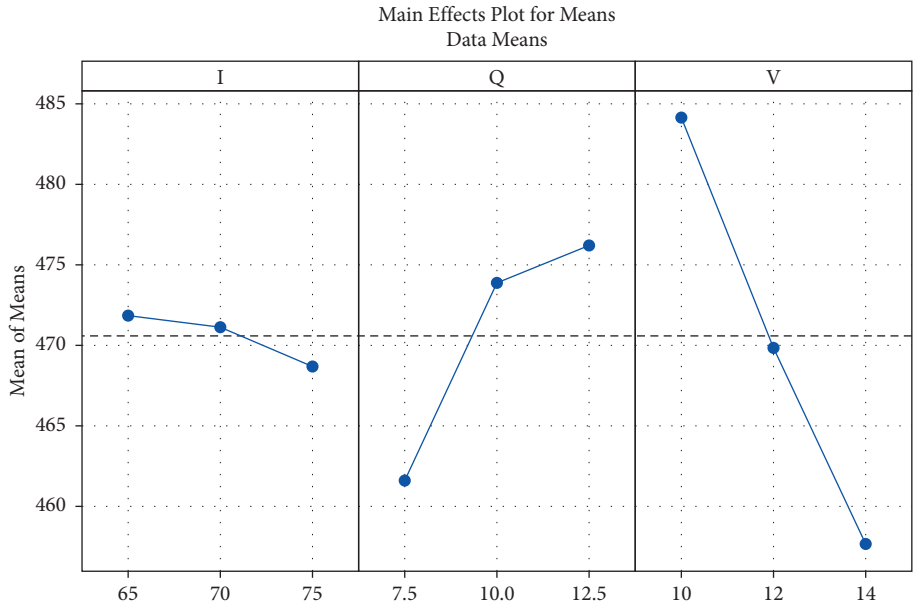

Figure 10: Main effects plot for means.

Table 6: Analysis of variance for tensile strength.

Source	DF	Adj SS	Adj MS	*F* value	*P* value	% contribution
Regression	3	1397.58	465.86	10.00	0.015	
Welding current	1	15.04	15.04	0.32	0.594	0.92
Gas flow rate	1	321.20	321.20	6.89	0.047	19.69
Welding voltage	1	1061.34	1061.34	22.78	0.005	65.09
Error	5	232.95	46.59			14.28
Total	8	1630.53				

Table 7: Model summary for tensile strength.

S	R-sq (%)	R-sq (adj) (%)	R-sq (pred) (%)
6.82562	85.71	77.14	41.38

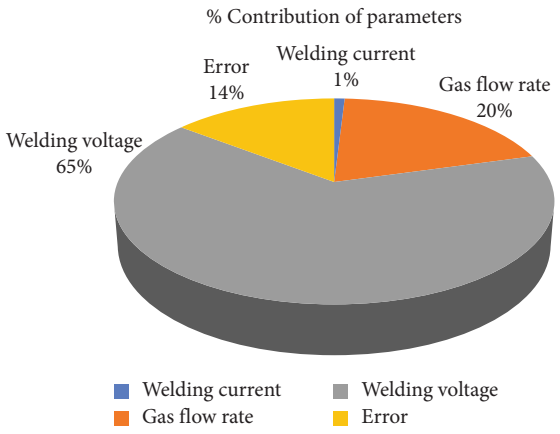

Figure 11: % contribution of parameters for tensile strength.

heat on the specimen. An optical microscope with a magnification of 200*x* was employed. Figure 12 shows the three primary microstructure zones of specimens 3 and 6, i.e.,

Table 8: Normalized values for the output response.

Run order	Microhardness (HV)	Tensile strength (MPa)
1	1.000	0.594
2	0.895	0.583
3	0.789	0.556
4	0.509	0.488
5	0.596	0.276
6	0.719	0.918
7	0.000	0.000
8	0.386	1.000
9	0.228	0.533

Table 9: Grey relation analysis result.

	GRC values			
Run order	Microhardness (HV)	Tensile strength (MPa)	GRG	Rank
1	1.000	0.552	0.776	1
2	0.826	0.545	0.686	4
3	0.704	0.530	0.617	5
4	0.504	0.494	0.499	6
5	0.553	0.408	0.481	7
6	0.640	0.859	0.750	2
7	0.333	0.333	0.333	9
8	0.449	1.000	0.724	3
9	0.393	0.517	0.455	8

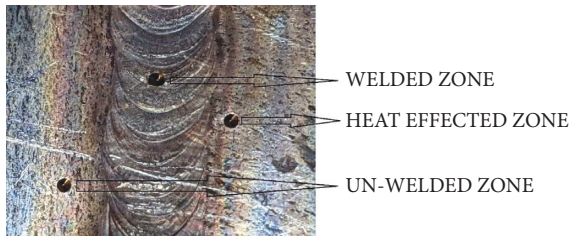

Figure 12: Zones of welded sheet.

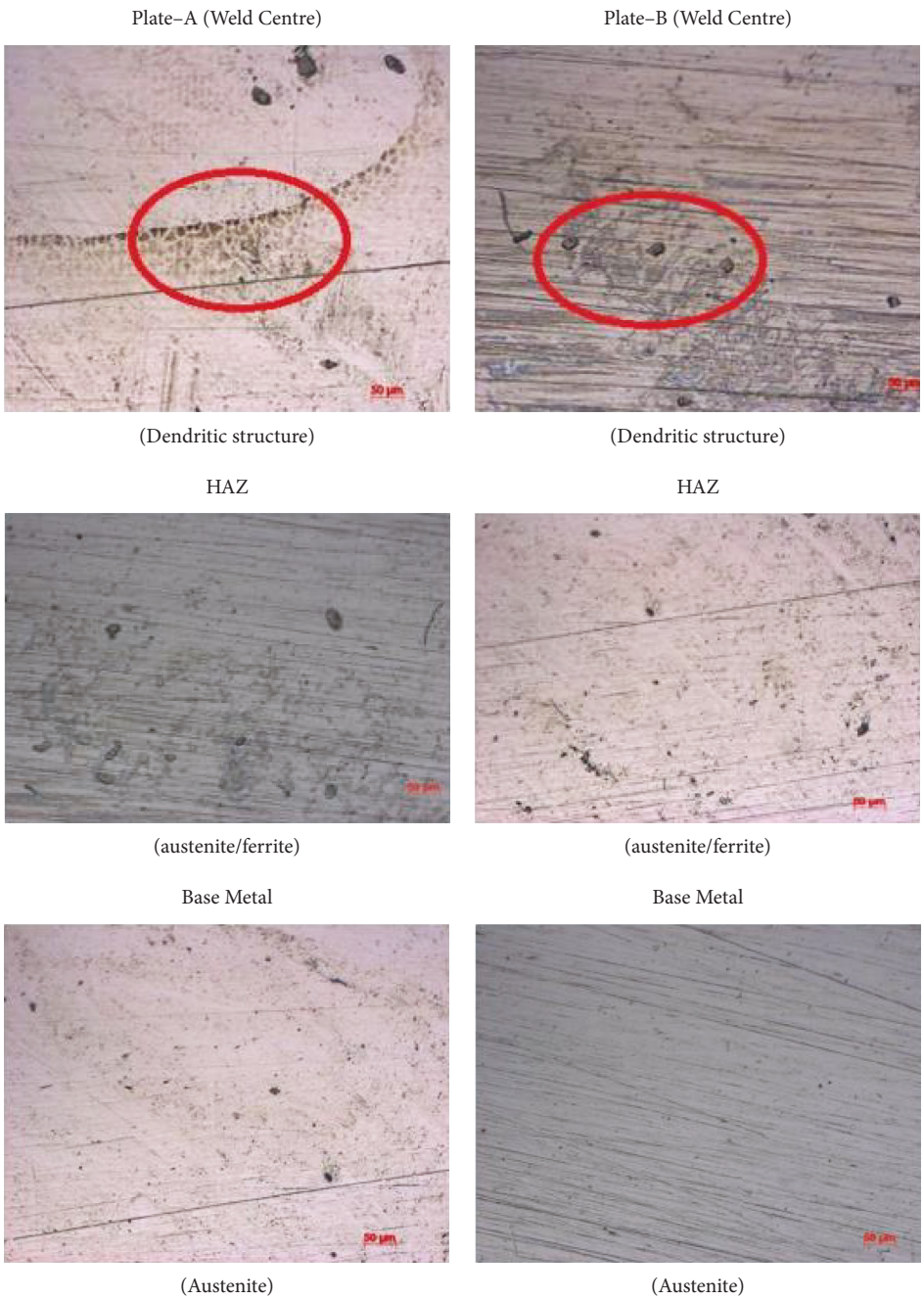

Figure 13: Microstructure analysis of welded specimens.

heat-affected zone (HAZ), weld zone, and base metal structure, respectively. The obtained image is presented in Figure 12. The predominant microstructural constituent created during the solidification process of iron-based alloys weld is dendritic microstructure. The rapid migration of the liquid/solid boundary towards the undercooled melt causes rapid dendritic development. In HAZ, it is possible that the dark microstructure is related to the after high-temperature welding and the existence of delta ferrite in the material.

The mechanical qualities of a weld are directly affected by changes in microstructure. As a result, when the heat input is large, the welded joint's hardness drops significantly due to microstructure coarsening. Figure 13 shows the optical analysis of the welded specimens.

6. Conclusion

The 310 SS TIG welding experimental study yielded positive results. Experiments were performed to analyze hardness, and tensile tests and optical analysis were carried out with precision to limit the mistake to a minimum and accurately identify the results. The DOE methodology and grey relation analysis techniques were used to optimize the TIG welding process parameters. The following conclusions were observed.

(a) For the specimen investigated, a welding current of 65 A and voltage of 10 V produced greater tensile strength, while a welding current of 75 A and voltage of 10 V produced the lowest tensile strength.

(b) The optimum parameter was set in GRA, and DOE was discovered to be outside the L9 experimental run. DOE predicted a lower value for the proximity coefficient than GRA's grey relational grade value.

(c) When comparing the parameter sets acquired via GRA and DOE, it was discovered that the parameter set obtained from GRA was closer to the experimental results.

(d) Due to the moderate cooling rate and high energy density of tungsten inert welding, microhardness studies revealed that the weldment zone had higher microhardness than normal.

(e) Microstructure changes have a direct impact on a weld's mechanical characteristics. When the heat input is significant, the welded joint's hardness drops dramatically as a result of the coarsening of the microstructure.

(f) The future work can also be performed by using advanced alloys such as Inconel by adopting other optimization techniques such as artificial neural network and response surface methodology.

Data Availability

All data generated or analyzed during this study are included in this article.

Conflicts of Interest

The authors declare no conflicts of interest with respect to research, authorship, and/or publication of this article.

Authors' Contributions

Conceptualization, writing, and original draft were carried out by A. G. and H. K.; methodology was performed by J. L. and K. K. S.; review and editing were carried out by K. A. M. and N. U. S.

Acknowledgments

The authors would like to acknowledge the support of Material Research Centre, Malviya National Institute of Technology, Jaipur (MNIT), for providing the facilities for hardness test and optical analysis of the specimens.

References

[1] P. K. Sarkar and S. K. Kakoty, "Pareto optimization of TIG welding process for joining the bell metal," *Materials and Manufacturing Processes*, vol. 37, no. 8, pp. 956–964, 2021.

[2] T. Sathish, S. Tharmalingam, V. Mohanavel et al., "Weldability investigation and optimization of process variables for TIG-welded aluminium alloy (AA 8006)," *Advances in Materials Science and Engineering*, vol. 2021, pp. 1–17, 2021.

[3] W. Chuaiphan and L. Srijaroenpramong, "Optimization of TIG welding parameter in dissimilar joints of low nickel stainless steel AISI 205 and AISI 216," *Journal of Manufacturing Processes*, vol. 58, pp. 163–178, 2020.

[4] N. Sharma, W. Sleam Abduallah, M. Garg, R. Dev Gupta, R. Khanna, and R. Chandmal Sharma, "Optimization of TIG welding parameters for the 202 stainless steel using NSGA-II," *Journal of Engineering Research*, vol. 8, no. 4, 2020.

[5] A. R. Pavan, N. Chandrasekar, B. Arivazhagan, S. Kumar, and M. Vasudevan, "Study of arc characteristics using varying shielding gas and optimization of activated-tig welding technique for thick AISI 316L (N) plates," *CIRP Journal of Manufacturing Science and Technology*, vol. 35, pp. 675–690, 2021.

[6] Z. Wan, D. Meng, Y. Zhao et al., "Improvement on the tensile properties of 2219-T8 aluminum alloy TIG welding joint with weld geometry optimization," *Journal of Manufacturing Processes*, vol. 67, pp. 275–285, 2021.

[7] M. Azadi Moghaddam and F. Kolahan, "Optimization of A-TIG welding process using simulated annealing algorithm," *Journal of Advanced Manufacturing Systems*, vol. 19, no. 04, pp. 869–891, 2020.

[8] D. Pandya, A. Badgujar, and N. Ghetiya, "A novel perception toward welding of stainless steel by activated TIG welding: a review," *Materials and Manufacturing Processes*, vol. 36, no. 8, pp. 877–903, 2021.

[9] A. Balaram Naik and A. Chennakeshava Reddy, "Optimization of tensile strength in TIG welding using the Taguchi method and analysis of variance (ANOVA)," *Thermal Science and Engineering Progress*, vol. 8, pp. 327–339, 2018.

[10] M. Ragavendran, N. Chandrasekhar, R. Ravikumar, R. Saxena, M. Vasudevan, and A. K. Bhaduri, "Optimization of hybrid

laser–TIG welding of 316LN steel using response surface methodology (RSM)," *Optics and Lasers in Engineering*, vol. 94, pp. 27–36, 2017.

[11] R. S. Vidyarthy, D. K. Dwivedi, and V. Muthukumaran, "Optimization of A-TIG process parameters using response surface methodology," *Materials and Manufacturing Processes*, vol. 33, no. 7, pp. 709–717, 2018.

[12] P. Vasantharaja and M. Vasudevan, "Optimization of A-TIG welding process parameters for RAFM steel using response surface methodology," *Proceedings of the Institution of Mechanical Engineers-Part L: Journal of Materials: Design and Applications*, vol. 232, no. 2, pp. 121–136, 2018.

[13] R. Pamnani, M. Vasudevan, P. Vasantharaja, and T. Jayakumar, "Optimization of A-GTAW welding parameters for naval steel (DMR 249 A) by design of experiments approach," *Proceedings of the Institution of Mechanical Engineers-Part L: Journal of Materials: Design and Applications*, vol. 231, no. 3, pp. 320–331, 2017.

[14] P. K. Singh, S. D. Kumar, D. Patel, and S. B. Prasad, "Optimization of vibratory welding process parameters using response surface methodology," *Journal of Mechanical Science and Technology*, vol. 31, no. 5, pp. 2487–2495, 2017.

[15] G. Magudeeswaran, S. R. Nair, L. Sundar, and N. Harikannan, "Optimization of process parameters of the activated tungsten inert gas welding for aspect ratio of UNS S32205 duplex stainless steel welds," *Defence technology*, vol. 10, no. 3, pp. 251–260, 2014.

[16] P. Sivachidambaram and K. Balachandar, "Optimization of pulsed current TIG welding parameters on al-sic metal matrix composite-An empirical approach," *Indian Journal of Science and Technology*, vol. 8, no. 23, p. 1, 2015.

[17] P. S. Lugade and M. J. Deshmukh, "Optimization of process parameters of activated tungsten inert gas (A-TIG) welding for stainless steel 304L using Taguchi method," *International Journal of Engineering Research and General Science*, vol. 3, no. 3, pp. 854–860, 2015.

[18] R. Adalarasan and M. Santhanakumar, "Parameter design in fusion welding of AA 6061 aluminium alloy using desirability grey relational analysis (DGRA) method," *Journal of the Institution of Engineers: Series C*, vol. 96, no. 1, pp. 57–63, 2015.

[19] K. A. Bello, M. A. Maleque, Z. Ahmad, and S. Mridha, "Optimization of hardness behaviour of TIG modified ceramic coating using the Taguchi approach," *Advanced Materials Research*, vol. 1115, pp. 238–242, 2015.

[20] N. Kiaee and M. Aghaie-Khafri, "Optimization of gas tungsten arc welding process by response surface methodology," *Materials & Design*, vol. 54, pp. 25–31, 2014.

[21] E. Rastkerdar, M. Shamanian, and A. Saatchi, "Taguchi optimization of pulsed current GTA welding parameters for improved corrosion resistance of 5083 aluminum welds," *Journal of Materials Engineering and Performance*, vol. 22, no. 4, pp. 1149–1160, 2013.

[22] M. P. Chakravarthy, N. Ramanaiah, and B. S. S. Rao, "Process parameters optimization for pulsed TIG welding of 70/30 Cu-Ni alloy welds using Taguchi technique," *International Journal of Mechanical & Mechatronics Engineering*, vol. 7, no. 4, pp. 763–769, 2014.

[23] H. L. Lin, "Optimization of Inconel 718 alloy welds in an activated GTA welding via Taguchi method, gray relational analysis, and a neural network," *International Journal of Advanced Manufacturing Technology*, vol. 67, no. 1-4, pp. 939–950, 2013.

[24] A. Goyal and H. Ur Rahman, "Experimental studies on Wire EDM for surface roughness and kerf width for shape memory alloy," *Sādhanā*, vol. 46, no. 3, pp. 160–213, 2021.

[25] D. Bandhu, J. J. Vora, S. Das et al., "Experimental study on application of gas metal arc welding based regulated metal deposition technique for low alloy steel," *Materials and Manufacturing Processes*, pp. 1–19, 2022.

[26] A. Goyal, D. Sharma, A. Bhowmick, and V. K. Pathak, "Experimental investigation for minimizing circularity and surface roughness under nano graphene mixed dielectric EDM exercising fuzzy-ANFIS approach," *International Journal on Interactive Design and Manufacturing*, vol. 16, no. 3, pp. 1135–1154, 2022.

[27] D. R. Tripathi, K. H. Vachhani, D. Bandhu, S. Kumari, V. R. Kumar, and K. Abhishek, "Experimental investigation and optimization of abrasive waterjet machining parameters for GFRP composites using metaphor-less algorithms," *Materials and Manufacturing Processes*, vol. 36, no. 7, pp. 803–813, 2021.

[28] D. Sharma, A. Bhowmick, and A. Goyal, "Enhancing EDM performance characteristics of Inconel 625 superalloy using response surface methodology and ANFIS integrated approach," *CIRP Journal of Manufacturing Science and Technology*, vol. 37, pp. 155–173, 2022.

[29] G. S. Kumar, M. Ramesh, S. Dinesh, P. Paramasivam, and N. Parthipan, "Investigation of the TIG welding process for joining AA6082 alloy using grey relational analysis," *Advances in Materials Science and Engineering*, vol. 2022, pp. 1–8, Article ID 5670172, 2022.